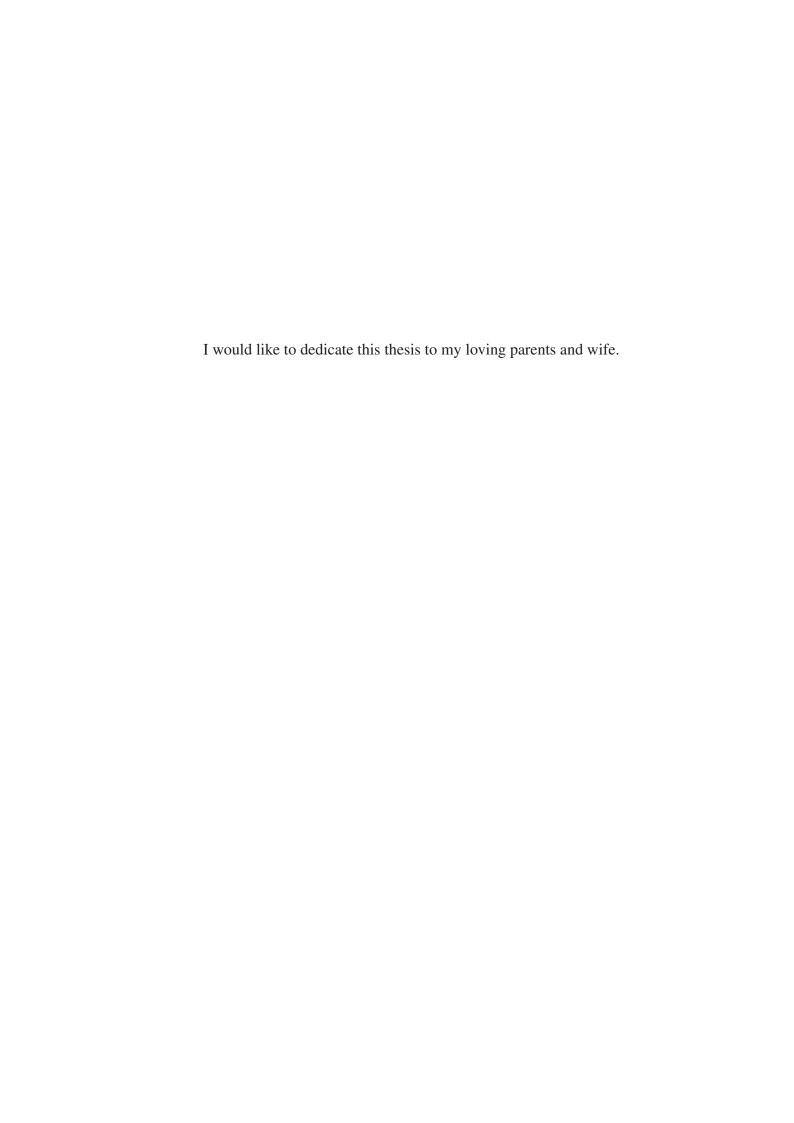
Robust Graph Transduction



Chen Gong

Centre for Quantum Computation & Intelligent Systems
University of Technology, Sydney

A thesis submitted for the degree of Doctor of Philosophy May, 2016



Acknowledgements

I would like to express my gratitude to all those who helped me during the writing of this thesis.

My deepest gratitude goes first and foremost to my supervisor Prof. Dacheng Tao, for his patient and valuable guidance. I knew little about research when I began my PhD study in UTS. It was Prof. Dacheng Tao who taught me how to find interesting ideas, how to develop solid algorithms, and how to write technical papers all from scratch. He was always ready to help, and was very willing to teach everything he knows to me. Without his illuminating instructions, insightful inspiration, consistent encouragement, and expert guidance, I would not have published papers on the leading journals or conferences in my research field. Therefore, I feel extremely grateful for Prof. Dacheng Tao's effort.

I am also greatly indebted to the Centre for Quantum Computation & Intelligent Systems (QCIS) directed by Prof. Chengqi Zhang. In QCIS, I got the opportunities to learn from many world-famous experts; I met many colleagues with great enthusiasm for scientific research; and I was also permitted to attend many prestigious international conferences related to my research. Studying in QCIS and also UTS will be a fantastic memory that I will never forget.

I would also like to thank Prof. Jie Yang from Shanghai Jiao Tong University. Without his introduction, I would not have the opportunity to study in UTS under the supervision of Prof. Dacheng Tao.

Last but not the least, my gratitude also extends to my family who have been consistently supporting, encouraging and caring for me all of my life!

Abstract

Given a weighted graph, graph transduction aims to assign unlabeled examples explicit class labels rather than build a general decision function based on the available labeled examples. Practically, a dataset usually contains many noisy data, such as the "bridge points" located across different classes, and the "outliers" that incur abnormal distances from the normal examples of their classes. The labels of these examples are usually ambiguous and also difficult to decide. Labeling them incorrectly may further bring about erroneous classifications on the remaining unlabeled examples. Therefore, their accurate classifications are critical to obtaining satisfactory final performance.

Unfortunately, current graph transduction algorithms usually fall short of tackling the noisy but critical examples, so they may become fragile and produce imperfect results sometimes. Therefore, in this thesis we aim to develop a series of robust graph transduction methodologies via iterative or non-iterative way, so that they can perfectly handle the difficult noisy data points. Our works are summarized as follows:

In Chapter 2, we propose a robust non-iterative algorithm named "Label Prediction via Deformed Graph Laplacian" (LPDGL). Different from the existing methods that usually employ a traditional graph Laplacian to achieve label smoothness among pairs of examples, in LPDGL we introduce a deformed graph Laplacian, which not only induces the existing pairwise smoothness term, but also leads to a novel local smoothness term. This local smoothness term detects the ambiguity of each example by exploring the associated degree, and assigns confident labels to the examples with large degree, as well as allocates "weak labels" to the uncertain examples with small degree. As a result, the negative effects of outliers and bridge points are suppressed, leading to more robust transduction performance than some existing representative algorithms. Although LPDGL is designed for transduction purpose, we show that it can be easily extended to inductive settings.

In Chapter 3, we develop an iterative label propagation approach, called "Fick's Law Assisted Propagation" (FLAP), for robust graph transduction.

To be specific, we regard label propagation on the graph as the practical fluid diffusion on a plane, and develop a novel label propagation algorithm by utilizing a well-known physical theory called Fick's Law of Diffusion. Different from existing machine learning models that are based on some heuristic principles, FLAP conducts label propagation in a "natural" way, namely when and how much label information is received or transferred by an example, or where these labels should be propagated to, are naturally governed. As a consequence, FLAP not only yields more robust propagation results, but also requires less computational time than the existing iterative methods.

In Chapter 4, we propose a propagation framework called "Teachingto-Learn and Learning-to-Teach" (TLLT), in which a "teacher" (i.e. a teaching algorithm) is introduced to guide the label propagation. Different from existing methods that equally treat all the unlabeled examples, in TLLT we assume that different examples have different classification difficulties, and their propagations should follow a simple-to-difficult sequence. As such, the previously "learned" simple examples can ease the learning for the subsequent more difficult examples, and thus these difficult examples can be correctly classified. In each iteration of propagation, the teacher will designate the simplest examples to the "learner" (i.e. a propagation algorithm). After "learning" these simplest examples, the learner will deliver a learning feedback to the teacher to assist it in choosing the next simplest examples. Due to the collaborative teaching and learning process, all the unlabeled examples are propagated in a well-organized sequence, which contributes to the improved performance over existing methods.

In Chapter 5, we apply the TLLT framework proposed in Chapter 4 to accomplish saliency detection, so that the saliency values of all the superpixels are decided from simple superpixels to more difficult ones. The difficulty of a superpixel is judged by its informativity, individuality, inhomogeneity, and connectivity. As a result, our saliency detector generates manifest saliency maps, and outperforms baseline methods on the typical public datasets.

Contents

Co	ontent	S	V
Li	st of l	ligures	viii
Li	st of T	Cables	xiii
1	Intr	oduction	1
	1.1	Background	1
	1.2	Related Work	5
		1.2.1 Non-iterative Methods	6
		1.2.2 Iterative Methods	8
	1.3	Motivations and Contributions	9
	1.4	Thesis Structure	13
	1.5	Publications during PhD Study	14
2	Lab	el Prediction Via Deformed Graph Laplacian	16
	2.1	Transduction In Euclidean Space	18
		2.1.1 Sensitivity of γ	21
		2.1.2 Sensitivity of β	22
	2.2	Induction In RKHS	22
		2.2.1 Robustness Analysis	23
		2.2.2 Generalization Risk	26
		2.2.3 Linearization of Kernelized LPDGL	27
	2.3	Relationship Between LPDGL and Existing Methods	29
	2.4	Experiments	31
		2.4.1 Toy Data	31
		2.4.1.1 Transduction on 3D Data	31
		2.4.1.2 Visualization of Generalizability	32
		2.4.2 Real Benchmark Data	33
		2.4.3 UCI Data	34
		2.4.4 Handwritten Digit Recognition	39

CONTENTS

		2.4.5 Face Recognition	40
		2.4.5.1 <i>Yale</i>	40
		2.4.5.2 <i>LFW</i>	42
		2.4.6 Violent Behavior Detection	43
	2.5	Summary of This Chapter	45
3	Fick	T. G.	46
	3.1	1	47
	3.2	e ,	50
	3.3	1	53
		3.3.1 Regularization Networks	53
		3.3.2 Markov Random Fields	54
		3.3.3 Graph Kernels	56
	3.4	Experimental Results	56
			57
		3.4.2 Real Benchmarks Data	59
		3.4.3 UCI Data	61
		3.4.4 Handwritten Digit Recognition	62
		3.4.5 Teapot Image Classification	64
			64
		3.4.7 Statistical Significance	65
			66
			67
			67
		3.4.9.2 Choosing K	69
	3.5		70
4	Lab	el Propagation Via Teaching-to-Learn and Learning-to-Teach	74
	4.1	A Brief Introduction to Machine Teaching	75
	4.2		76
	4.3	Teaching-to-Learn Step	77
		4.3.1 Curriculum Selection	78
			81
	4.4	<u>-</u>	83
	4.5		86
			86
		a contract of the contract of	87
	4.6		88
	4.7	•	92
	4.8		- 94
		1	o. 94

CONTENTS

		4.8.2	UCI Benchmark Data	96
		4.8.3	Text Categorization	97
		4.8.4	Object Recognition	98
		4.8.5	Fine-grained Image Classification	99
		4.8.6		100
	4.0		Parametric Sensitivity	
	4.9	Summ	ary of This Chapter	101
5	Teac	ching-to	-Learn and Learning-to-Teach For Saliency Detection	103
	5.1	_	ef Introduction to Saliency Detection	103
	5.2		cy Detection Algorithm	105
		5.2.1	Image Pre-processing	106
		5.2.2	Coarse Map Establishment	107
		5.2.3	Map Refinement	107
	5.3		ng-to-learn and Learning-to-teach For Saliency Propagation	108
		5.3.1	Teaching-to-learn	108
		5.3.2	Learning-to-teach	111
		5.3.3	Saliency Propagation	113
	5.4		mental Results	114
	5.1	5.4.1	Experiments on Public Datasets	114
		5.4.2	Parametric Sensitivity	117
		5.4.3	Failed Cases	117
	5.5		ary of This Chapter	119
	3.3	Summ	ary or rins chapter	11)
6	Con	clusion	and Future Work	120
	6.1	Thesis	Summarization	120
	6.2	Relation	onship and Differences among Algorithms	121
	6.3		Work	122
Re	eferen	ces		124

List of Figures

1.1	The illustration of graph, where the circles represent the vertices $\mathbf{x}_1 \sim \mathbf{x}_7$ and the lines are edges. The red circle denotes the positive example with label 1, while blue circle denotes the negative example with label -1. The numbers near the edges are weights evaluating the similarity	
1.2	between the two connected vertices	10
1.3	respectively	10 14
2.1	The illustration of local smoothness constraint on <i>DoubleLine</i> dataset. A k -NN graph with $k=2$ is built and the edges are shown as green lines in (a). (b) shows the result without incorporating the local smoothness, and (c) is the result produced by the proposed LPDGL. The labels of "bridge point" under two different simulations are highlighted in (b) and (c), respectively	17
2.2	The evolutionary process from LPDGL to other typical SSL methods. The dashed line means "infinitely approach to". Note that our LPDGL is located in the central position and other algorithms are derived from LPDGL by satisfying the conditions alongside the arrows.	29
2.3	Transduction on two 3D datasets: (a) and (d) show the initial states of <i>Cylinder&Ring</i> and <i>Knot</i> , respectively, in which the red triangle denotes a positive example and the blue circle represents a negative example. (b) and (e) are the transduction results of developed LPDGL	
	on these two datasets. (c) and (f) present the results of LPDGL (Linear).	32

2.4	Induction on <i>DoubleMoon</i> and <i>Square&Ring</i> datasets. (a) and (d) show the initial states with the marked labeled examples. (b) and (e) are induction results, in which the decision boundaries are plotted. (c)	
2.5	and (f) are induction performances produced by LPDGL (Linear) Experimental results on four UCI datasets. (a) and (e) are <i>Iris</i> , (b) and (f) are <i>Wine</i> , (c) and (g) are <i>BreastCancer</i> , and (d) and (h) are <i>Seeds</i> . The sub-plots in the first row compare the transductive performance of the algorithms, and the sub-plots in the second row compare their	33
2.6	inductive performance	34
2.7	results, and the sub-plots in the second row display the inductive results. Experimental results on <i>USPS</i> dataset. (a) shows the transductive results, and (b) shows the inductive results	37
3.1	The parallel between fluid diffusion and label propagation. The left cube with more balls is compared to the example with more label information. The right cube with fewer balls is compared to the example with less label information. The red arrow indicates the	
3.2	diffusion direction	48 58
3.3	The propagation results on <i>DoubleMoon</i> dataset. (a), (b), (c) are propagation processes of FLAP, LGC and LNP, respectively. (d), (e), (f) present the classification results brought by MinCut, HF and NTK.	59
3.4	The comparison of convergence curves. (a) is the result on <i>Square&Ring</i> and (b) is that on <i>DoubleMoon</i>	60
3.5	Classification outputs on imbalanced <i>DoubleMoon</i> . (a), (b), (c) and (d) are results of 1:2, 1:5, 1:10 and 1:25 situations, respectively	61
3.6	Comparison of accuracy and iteration times. (a) (b) denote <i>Iris</i> , (c) (d) denote <i>Wine</i> , (e) (f) denote <i>BreastCancer</i> , and (g) (h) denote <i>CNAE-9</i> .	63
3.7	Comparison of accuracy and iteration times on digit recognition dataset. (a), (b) are the curves of accuracy and iteration times with	0.
3.8	the growing of the labeled examples, respectively	64
3.9	the accuracy curve for comparison	65
	tive images, and (b) compares the recognition accuracy	66

3.	10 Distribution of eigenvalues on <i>Iris</i> . (a) denotes LNP, (b) denotes LGC and (c) denotes FLAP. Note that the ranges of the three x-axes are	70
3.	different	70 71
4.	unlabeled examples, and curriculum are represented by red, grey, and green balls, respectively. The steps of Teaching-to-Learn and Leaning-to-Teach are marked with blue and black dashed boxes	76
4.	2 The toy example to illustrate our motivation. The orientation (left or right) of the spout in each image is to be determined. Labeled positive and negative examples are marked with red and blue boxes, respectively. The difficulties of these examples are illustrated by the two arrows below the images. The propagation sequence generated by the conventional methods Gong et al. [2014b]; Zhou and Bousquet [2003]; Zhu and Ghahramani [2002] is {1,6} → {2,3,4,5}, while TLLT operates in the sequence {1,6} → {2,5} → {3} → {4}. As a consequence, only the proposed TLLT can correctly classify the most	
4.	difficult images 3 and 4	77
	information to the simple vertex \mathbf{x}_C	92

4.4	The propagation process of the methods on the <i>DoubleMoon</i> dataset. (a) is the initial state with marked labeled examples and difficult bridge point. (b) shows the imperfect edges during graph construction caused by the bridge point in (a). These unsuitable edges pose a difficulty for all the compared methods to achieve accurate propagation. The second row $(c)\sim(i)$ shows the intermediate propagations of TLLT (Norm), TLLT (Entropy), GFHF, LGC, LNP, DLP, and GTAM. The third row $(j)\sim(p)$ compares the results achieved by all the algorithms, which reveals that only the proposed TLLT achieves perfect classification	
4.5 4.6	while the other methods are misled by the ambiguous bridge point Example images of <i>COIL20</i> dataset	95 98 99
4.7	Parametric sensitivity of TLLT. The first, second and third rows correspond to $RCVI$, $COIL20$ and UT $Zappos$ datasets, respectively. (a), (c) and (e) show the variation of accuracy w.r.t. the kernel width ξ when α is fixed to 1, and (b), (d) and (f) evaluate the influence of the trade-off α to final accuracy under $\xi = 10. \dots \dots$.	102
5.1	The results achieved by typical propagation methods and our method on two example images. From left to right: input images, results of Yang et al. [2013b], Jiang et al. [2013], and our method.	104
5.2	The diagram of our detection algorithm. The magenta arrows annotated with numbers denote the implementations of teaching-to-learn	
5.3	and learning-to-teach propagation shown in Fig. 5.3 An illustration of our teaching-to-learn and learning-to-teach paradigm. In the teaching-to-learn step, based on a set of labeled superpixels (magenta) in an image, the teacher discriminates the adjacent unlabeled superpixels as difficult (blue superpixels) or simple (green superpixels) by fusing their informativity, individuality, inhomogeneity, and connectivity. Then simple superpixels are learned by the learner, and the labeled set is updated correspondingly. In the learning-to-teach step, the learner provides a learning feedback to the teacher to help decide	106
5.4	the next curriculum	109
	region s_1 in (a) obtains larger individuality than s_2 , and s_3 in (b) is more inhomogeneous than s_4 .	112

5.5	Visualization of the designed propagation process. (a) shows the input	
	image with boundary seeds (yellow). (b) displays the propagations	
	in several key iterations, and the expansions of labeled set $\mathcal L$ are	
	highlighted with light green masks. (c) is the final saliency map. The	
	curriculum superpixels of the 2nd iteration decided by informativity,	
	individuality, inhomogeneity, connectivity, and the final integrated	
	result are visualized in (d), in which the magenta patches represent	
	the learned superpixels in the 1st propagation, and the regions for the	
	2nd diffusion are annotated with light green	113
5.6	Comparison of different methods on two saliency detection datasets.	
	(a) is MSRA 1000, and (b) is ECSSD	115
5.7	Visual comparisons of saliency maps generated by all the methods on	
	some challenging images. The ground truth (GT) is presented in the	
	last column	116
5.8	Parametric sensitivity analyses: (a) shows the variation of F_{β}^{w} w.r.t. θ	
	by fixing $N=400$; (b) presents the change of F_{β}^{w} w.r.t. N by keeping	
	$\theta = 0.25.$	117
5.9	Failed cases of our method. (a) shows an example that the object is	
	very similar to the background, in which the correct seed superpixels	
	are marked with magenta. (b) is the imperfect saliency map corre-	
	sponding to the image in (a). In (c), the targets are completely missed	
	by the convex hull (blue polygon), which leads to the detection failure	
	as revealed by (d)	118

List of Tables

2.1	Experimental results on the benchmark datasets for the variety of	
	transduction algorithms. (The values in the table represent the error	
	rate (%). The best three results for each dataset are marked in red,	
	blue, and green, respectively.)	35
2.2	Summary of four UCI datasets	36
2.3	F-statistics values of inductive algorithms versus LPDGL on UCI	
	datasets. (The records smaller than 4.74 are marked in red, which mean	
	that the null hypothesis is accepted.)	38
2.4	Transductive comparison on <i>Yale</i> dataset	41
2.5	Inductive comparison on <i>Yale</i> dataset	41
2.6	Transductive comparison on <i>LFW</i> dataset	42
2.7	Inductive comparison on <i>LFW</i> dataset	43
2.8	Transductive results on <i>HockeyFight</i> dataset	44
2.9	Inductive results on <i>HockeyFight</i> dataset	44
3.1	FLAP vs. popular graph transduction algorithms	55
3.2	Performances of all the methods on two synthetic datasets. Each record	
	follows the format "iteration time/CPU seconds/accuracy"	57
3.3	Experimental results on the benchmark datasets for the variety of graph	
	transduction algorithms. (The values in the table represent accuracy (%).)	62
3.4	F-statistics values of baselines versus FLAP on four UCI datasets.	
	(The records smaller than 4.74 are marked in red, which mean that	
	1) the null hypothesis is accepted, and 2) the corresponding baseline	
	algorithm performs comparably to FLAP.)	72
3.5	CPU time (unit: seconds) of various methods. (For each l , the smallest	
	record among iterative methods is marked in red, while the smallest	
	record among non-iterative methods is highlighted in blue.)	73

LIST OF TABLES

4.1	Experimental results of the compared methods on four UCI benchmark	
	datasets. (Each record in the table represents the "accuracy \pm standard	
	deviation". The highest result obtained on each dataset is marked in	
	bold.)	97
4.2	Accuracy of all methods on the RCVI dataset (the highest records are	
	marked in bold)	98
4.3	Accuracy of all methods on the COIL20 dataset (the highest records	
	are marked in bold)	99
4.4	Accuracy of all methods on UT Zappos dataset (highest records are	
	marked in bold)	100
5.1	Average CPU seconds of all the approaches on ECSSD dataset	116